The threshold for continuing saltation on Earth and other solar system bodies

Diego Berzi, Alexandre Valance, Jim T. Jenkins

The threshold for continuing saltation on Earth and other Solar System bodies

D. Berzi[1], A. Valance[2], and J. T. Jenkins[3]

[1] Department of Civil and Environmental Engineering, Politecnico di Milano, 20133 Milano, Italy.

[2] Institut de Physique de Rennes, Université de Rennes I, 35042 Rennes, France.

[3] School of Civil and Environmental Engineering, Cornell University, Ithaca, NY 14850, USA.

Corresponding author: Diego Berzi (diego.berzi@polimi.it)

Key Points:

- Predicted threshold for continuing saltation explicitly accounting for densities, gravity and particle size
- Only one fitting parameter of order unity
- Successful comparisons against discrete numerical simulations and experiments in wind tunnels

This article has been accepted for publication and undergone full peer review but has not been through the copyediting, typesetting, pagination and proofreading process which may lead to differences between this version and the Version of Record. Please cite this article as doi: 10.1002/2016JF003982

Abstract

We predict the threshold for continuing saltation of spheres in a turbulent fluid that explicitly accounts for the influence of fluid drag, lubrication forces, bed roughness and inter-particle cohesion. This reduces the need for the fitting parameters employed in existing formulations. The theory is based on a highly idealized model of steady saltation as a collection of particles that follow the same average, periodic trajectory – a succession of identical jumps, collisions with the bed, and rebounds from it. The saltation threshold is first derived in the limit of large particle inertia and, then, extended to infer results when the viscous forces of the fluid and inter-particle cohesion are not negligible. The theory is successfully compared with existing discrete element simulations of spheres interacting with a Reynolds-averaged turbulent fluid and with wind tunnel experiments in a range of particle-to-fluid density ratios and particle Reynolds numbers for saltation in terrestrial and extra-terrestrial conditions.

1 Introduction

The interaction of flows of air or water with loose surface materials is responsible for many of the features in the geological record. An identification of the mechanisms involved in such interactions and the characterization of the influence that they have on initiating and maintaining sediment transport should permit a more subtle and refined reading of this record. In extra-terrestrial environments, a better understanding of particle transport driven by flows of gases and liquids allows more refined inferences about the conditions that generated features observed from afar. Here, we provide a quantitative, analytical description of a threshold for the maintenance of one mode of particle transport that incorporates the physical parameters that define the fluid flow and the interaction of the particles with the bed. Saltation – the motion of grains through successions of jumps induced by a shearing fluid, here considered turbulent – is known to be the principal mode of sediment transport by the wind on Earth [*Bagnold*, 1941; *Andreotti*, 2004; *Kok et al.*, 2012; *Charru et al.*, 2013; *Valance et al.*, 2015] and has been suggested to be relevant also for moderate sediment transport by water on Earth [*Fernandez Luque and Van Beek*, 1976; *Abbott and Francis*, 1977; *Niño and García*, 1998; *Ancey et al.*, 2002], although, in the latter case, interparticle collisions above the bed limit its importance [*Schmeeckle*, 2014; *Maurin et al.* 2016].

Saltation in air is usually a continuing process, in which a description of the fluid flow field in terms of its mean motion (e.g., Reynolds-averaged) is sufficient to explain why the particles move [*Sauermann et al.*, 2001; *Jenkins et al.*, 2010; *Durán et al.*, 2012; *Jenkins and Valance*, 2014]. In contrast, sediment transport in water, at least close to the threshold for motion, is usually described as intermittent and erratic, with turbulent fluctuations playing a significant role in moving particles [*Drake et al.*, 1988; *Nelson et al.*, 1995; *Lajeunesse et al.*, 2010]. However, it has been recently suggested [*Berzi et al.*, 2016] that there does exist a continuing saltation regime in aquatic sediment transport, although at intensities of the turbulent shearing larger than those usually encountered in laboratory experiments, but typical of some fluvial environments (such as sand-bed rivers). The prediction of continuing saltation in water on Earth at large intensities of turbulent shearing indicates that continuing saltation is likely to be the precursor to dense, collisional (sheet) flows. If so, continuing saltation provides the link between rolling, intermittent jumping, and sliding and sheet flows [*Gao*, 2008].The main difference between Aeolian and aquatic saltation on Earth is in the ratio of particle-to-fluid density: in the Aeolian case, the density ratio is of order 10^3, while in the aquatic case is of order 1. This has important consequences, for example, on the role of the collisions with the bed, or splash, [*Beladjine et al.*, 2007] in determining the flux of sediment from the bed [*Berzi et al.*, 2016].

Aeolian saltation on Earth is associated with the development of dunes [*Charru et al.*, 2013]. Because dunes have been observed on Mars, Venus [*Iversen and White*, 1982; *Greeley et al.*, 1984], and Titan [*Lorenz et al.*, 2006], a satellite of Saturn, it seems natural to assume that saltation is also relevant to these extra-terrestrial environments. Interestingly, in such situations, the density ratio is very different from the typical terrestrial values: it is roughly 40 on Venus, about 200 on Titan and of order 10^5 on Mars [*Iversen and White*, 1982; *Burr et al.*, 2015]. A large effort has been devoted to determine the wind speed necessary for the saltation process to initiate, and how this threshold is influenced by the planetary conditions. Establishing under what conditions saltation is possible could determine an Aeolian origin for the streaks, ripples and dunes observed on the surface of minor solar system bodies, such as moons, comets and asteroids [*Hansen et al.*, 1990; *Sagan and Chyba*, 1990; *Thomas et al.*, 2015]. The first formulation for this initiation threshold was based on considerations of rotational equilibrium of a sphere in contact with a surface under the effects of gravity and aerodynamic drag [*Bagnold*, 1941]; successive approaches have included the role of buoyancy [*Ward*, 1969], aerodynamic lift and inter-particle cohesive forces [*Ward*, 1969;

Iversen et al., 1976; *Iversen and White*, 1982; *Shao and Lu*, 2000], inter-particle impact force [*Iversen et al.*, 1987], and turbulent fluctuations [*Lu et al.*, 2005]. The resulting expressions for the threshold involve complicated functions of the particle Reynolds number at the threshold wind velocity, the density ratio, and the inter-particle cohesive forces. These must be obtained from fitting with experiments performed in wind tunnels that simulate terrestrial and extra-terrestrial conditions [*Iversen et al.*, 1976; *Greeley et al.*, 1984; *Burr et al.*, 2015]. Given that these approaches are meant to determine the wind speed at which a single particle begins to rotate, they actually describe the threshold for the initiation of rolling rather than that for continuing saltation. In the experiments of *Burr et al.* [2015], intended to reproduce the conditions on Titan, a threshold was identified as the value of wind speed at which there was a continuing motion along the central region of the longitudinal extent of the bed. Their measurement is consistent with the definition of continuing, or dynamic, saltation and explains why the expressions of *Shao and Lu* [2000] and *Iversen and White* [1982] for the initiation of rolling underpredicted the experimental data.

The threshold for continuing saltation coincides with the minimum fluid speed necessary to sustain the saltation process once it has started. This dynamic threshold has been the focus of many recent studies. *Andreotti* [2004] identified two species of particles, in the limit of large particle size, each characterized by a different constant trajectory (i.e., he assumed a constant slip velocity of the particles at the bed). He numerically solved for the particle motion and fit an expression for the dynamic threshold with three model parameters. *Claudin and Andreotti* [2006] extended the analysis of *Andreotti* [2004] to small particle size, including the force of cohesion, with a dynamic threshold that was to be determined through numerical integration of the equations of motion. In a different approach, *Kok* [2010] proposed a statistical model for the saltation threshold, assuming once again a constant slip velocity of the particles at the bed. He obtained an approximate expression for the threshold, which was the result of a fit to the numerical solution of the model, characterized by six dimensional parameters. Also *Pähtz et al.* [2012] assumed a constant particle slip velocity at the bed and proposed a physically based model of saltation with an analytical expression of the threshold that involved four parameters fit by experiments. Finally, *Pähtz and Durán* [2016] removed the assumption of constant slip velocity at the bed and replaced it with an assumption, motivated from numerical simulations, of a constant ratio of shear to normal particle stresses there. Then, using a phenomenological correlation between the particle and fluid horizontal velocities and the fluid shear stress, obtained from discrete element simulations, they provided an expression for the saltation threshold that included the role of particle size, cohesive forces, and the fluid rarefaction. This expression contains functions that need to be solved by iteration and four parameters obtained by fitting with simulations.

Jenkins and Valance [2014] modelled steady, continuing Aeolian saltation by imagining that all the particles follow the same trajectory between successive impacts with the bed, and that this trajectory, governed by gravity and fluid drag, is periodic. In the analysis, they solved for the trajectories numerically, making use of boundary conditions for the impact of a sphere with the bed derived from experiments [*Beladjine et al.*, 2007; *Crassous et al.*, 2007], without assuming either a constant slip velocity or a constant stress ratio for the particles at the bed. *Berzi et al.* [2016] extended the analysis to arbitrary values of the density ratio and provided analytical solutions for periodic trajectories over hydrodynamically rough beds (i.e., beds with roughness height larger than the thickness of the viscous sublayer). The family of periodic trajectories that satisfy the rebound boundary conditions were parametrized by the take-off velocity – the initial vertical velocity after the rebound. We emphasize that the model of *Jenkins and Valance* [2014] and *Berzi et al.* [2016] must be viewed as a simple, physically-based device to estimate how averages over the entire population of saltating particles, such as saltation lengths and heights and flow rate, are

related to the intensity of the shearing fluid in steady configurations. It is not meant to, and it does not, give realistic local distributions of velocities and volume concentration. The model of periodic trajectories cannot be employed in unsteady situations. In such situations, there is a net flux of particles to or from the bed and the averages above the bed are evolving. Each periodic trajectory is associated with a value of the fluid shear stress at the bed, determined as part of the solution. The fluid shear stress at the bed, which can be related to the take-off velocity, exhibits a minimum. This minimum is the smallest value of fluid shear stress at the bed that will maintain continuing saltation. *Berzi et al.* [2016] provide an explicit expression for this threshold, valid in the limit in which the particle inertia is large relative to the fluid viscous forces.

Here, we extend the analysis of *Berzi et al.* [2016] to deal with arbitrary values of particle inertia, explicitly accounting for non-linear drag, the influence of lubrication forces – the fluid viscous forces generated in the gap between two colliding spheres that reduce the interparticle impact force) in the impact with the bed, and particle motion over hydrodynamically smooth and transitional beds – that is beds with roughness heights less than or similar to the thickness of the viscous sublayer. We also include the role of inter-particle cohesion in the way suggested by *Shao and Lu* [2000]. The theory incorporates characterizations of the physical mechanisms that govern saltation and reduces the need for fitting parameters.

In Section 2, we present the analytical theory; in Section 3, we make comparisons with the saltation threshold obtained in numerical solutions for the periodic trajectories, discrete element simulations of spheres interacting with a continuum-averaged fluid [*Durán et al.*, 2012], and wind tunnel experiments [*Iversen and White*, 1982; *Burr et al.*, 2015].

2 Theory

We focus on steady, uniform, continuing saltation of spheres of diameter d and mass density ρ^s over a horizontal particle bed. A turbulent shearing flow of a fluid of mass density ρ^f and dynamic viscosity μ^f drives the flow in the presence of gravity, with g the gravitational acceleration. As in our previous works [*Jenkins and Valance*, 2014; *Berzi et al.*, 2016], we consider the average of the distribution of particle trajectories at a given strength of the turbulent shearing; in a steady situation, the average trajectory must be periodic. The horizontal and vertical particle velocities are u and v, respectively. Two coefficients of restitution characterize the impact of a particle with the bed and, if one neglects the role of lubrications forces, they are only a function of the angle of impact [*Oger et al.*, 2005; *Beladjine et al.*, 2007]. In an impact with the bed, e_y is the negative of the ratio of the particle vertical velocities after and before, and e is the ratio of the particle speeds after and before. For the saltation to continue, the mean horizontal velocity of the turbulent fluid, U, must be large enough to sustain the periodic motion. The flow configuration is depicted in Figure 1.

We characterize the particles through the fall particle Reynolds number $R = \rho^f \sqrt{g(\sigma-1)/\sigma}\, d^{3/2} / \mu^f$, where $\sigma = \rho^s/\rho^f$ is the density ratio. In what follows, all quantities are made dimensionless using the diameter and mass density of the particle and the reduced gravitational acceleration $g(\sigma\text{-}1)/\sigma$.

Given that the particles are subject to gravity, buoyancy, and fluid drag, assuming the usual logarithmic velocity profile for the turbulent fluid, and using the experimental dependence of the coefficients of restitution on the angle of impact, modified to incorporate the additional damping due to lubrications forces on binary collisions [*Barnocky and Davis*,

1988; *Gondret et al.*, 2002; *Yang and Hunt*, 2006], numerical solutions can be obtained for the periodic trajectories [*Jenkins and Valance*, 2014; *Berzi et al.*, 2016]. The differential equations governing the particle and fluid motion and the boundary conditions for these are briefly summarized in Appendix A. Other hydrodynamic forces such as lift, Magnus, added mass and Bassett forces [*Maxey and Riley*, 1983] are ignored in the analysis, given that their order of magnitude is that of the fluid drag divided by the dimensionless trajectory height [*Andreotti*, 2004], i.e., mostly negligible.

A simplified analytical solution to a periodic trajectory, in excellent agreement with the full numerical solution, can be obtained [*Berzi et al.*, 2016] by: ignoring the vertical drag; assuming a uniform, horizontal fluid velocity profile; and ignoring the vertical particle velocity in the expression of the drag coefficient (equation A1). An approximate integration of the logarithmic fluid velocity profile over the height, H, of the trajectory gives the fluid shear stress at the bed, S_0, in terms of the averaged fluid velocity, $\bar{U}$, as [*Berzi et al.*, 2016]:

$$S_0 = K \frac{\kappa^2}{\sigma \left[\ln\left(H / y_0 \right) \right]^2} \bar{U}^2, \tag{1}$$

where $\kappa = 0.41$ is von Kármán's constant, y_0 is the dimensionless roughness length, and K is a dimensionless numerical constant, taken equal to 1.5 by *Berzi et al.* [2016] based on a fit to the numerical solutions of the periodic trajectories. If the vertical drag is ignored, the y-component of the particle velocity is ballistic, and the trajectory height is simply

$$H = \frac{1}{2} v_i^2, \tag{2}$$

where v_i is the take-off velocity. Also the fluid depth-averaged velocity $\bar{U}$ is an increasing function of the take-off velocity [*Berzi et al.*, 2016]. Hence, both the numerator and the denominator of equation (1) are increasing functions of v_i and the fluid shear stress at the bed has a minimum at a critical value v_c of the take-off velocity. Given that the dimensionless particle shear stress is the difference between the dimensionless fluid shear stress far from the bed – the Shields parameter S^* – and the dimensionless local fluid shear stress, the minimum in S_0 corresponds also to the minimum Shields parameter for continuing saltation in the absence on inter-particle cohesion.

2.1 Limit of infinite particle inertia

We first calculate the critical Shields parameter in the limit of infinite particle inertia. This limit corresponds to large values of the particle Reynolds number R, for instance, large particle diameters for given particle and fluid properties. In this limit, the lubrication forces play no role in damping the rebound of the particle at the bed, so that e_y is simply equal to 1 – the vertical velocities before and after the impact, v_f and v_i, must have the same absolute value and opposite sign when the vertical drag is ignored and the trajectory is periodic – that is, $v_i = -v_f$. Hence, from equation (A15), the particle horizontal velocity before the impact is

$$u_f = \frac{1 + b_y}{a_y} v_i \equiv A v_i, \tag{3}$$

where, as explained in Appendix A, a_y and b_y are numerical constants determined in experiments on collisions with the bed. Similarly, neglecting the term inversely proportional to the Reynolds number in equation (A12) gives, with equation (3),

$$u_i = \left[e^2 u_f^2 + \left(e^2 - 1 \right) v_i^2 \right]^{1/2} = \left[e^2 A^2 + \left(e^2 - 1 \right) \right]^{1/2} v_i \equiv D v_i , \tag{4}$$

where, from equations (A14) and (3), $e \equiv a - b/A$, with a and be also experimentally determined numerical constants. In this work, we use $a_y = 0.30$, $b_y = 0.15$, $a = 0.87$ and $b = 0.72$ [*Beladjine et al.*, 2007].

Considering only the form drag in the particle horizontal momentum balance gives a relation between the fluid horizontal velocity and the particle horizontal velocities before and after impact (equation B3). Using equations (3) and (4) in equation (B3), and the fact that the time of flight in a ballistic trajectory is $t_f = 2 v_i$,

$$U = \frac{A + D}{2} v_i + \left(\frac{A - D}{0.6} \right)^{1/2} \sigma^{1/2} . \tag{5}$$

Employing equations (2) and (5) in equation (1), and requiring for an extremum that the derivative of S_0 with respect to the take-off velocity be equal to zero, determines the critical take-off velocity, v_c, for which the fluid shear stress at the bed is minimum,

$$v_c = \left[\frac{1}{2} \ln \left(\frac{15 v_c^2}{k_s} \right) - 1 \right]^{-1} \frac{2}{A + D} \left(\frac{A - D}{0.6} \right)^{1/2} \sigma^{1/2} . \tag{6}$$

In equation (6), we have used $y_0 = k_s / 30$ [*van Rijn*, 1984; *Jenkins and Valance*, 2014] – the roughness length for hydrodynamically rough beds, given that we are in the limit of large R [*Schlichting and Gersten*, 2000]. In this, k_s is the roughness, taken to be equal to one particle diameter [*Jenkins and Valance*, 2014].

Equation (6) is an implicit expression, which can be solved via iteration (for example, a successive substitution scheme or a Newton-Raphson method using $2^{1/2}$ as a first guess for the critical take-off velocity). An approximate, explicit solution can be obtained by expanding the logarithm in equation (6) about $v_c = 2^{1/2}$,

$$v_c \left[\frac{1}{2} \ln \left(\frac{15}{k_s} \right) - 1 + \frac{1}{2} \ln (2) + \frac{v_c - 2^{1/2}}{2^{1/2}} \right] = \frac{2}{A + D} \left(\frac{A - D}{0.6} \right)^{1/2} \sigma^{1/2} . \tag{7}$$

Equation (7) is a quadratic in the take-off velocity giving

$$v_c = -\alpha + \left(\alpha^2 + \beta \sigma^{1/2} \right)^{1/2} , \tag{8}$$

where $\alpha \equiv 2^{1/2} \left[\ln \left(15 / k_s \right) / 2 + \ln (2) / 2 - 2 \right] / 2$ and $\beta \equiv 2^{3/2} \left[(A - D) / 0.6 \right]^{1/2} / (A + D)$.

For a given set of numerical constants in the rebound law, the critical take-off velocity is a function only of the density ratio – equation (8) indicates that, for moderate to high density ratio, v_c is proportional to $\sigma^{1/4}$ – and so also is the critical Shields parameter. When σ is 2.5, as is the case for aquatic saltation on Earth, v_c is about $2^{1/2}$, so that the corresponding saltation height, from equation (2), would be roughly one particle diameter; when σ is 2500, as is the case for Aeolian saltation on Earth, v_c is about 5, so that the corresponding saltation height would be roughly 13 particle diameters. For larger density ratios, the take-off velocity predicted by equation (8) is larger than 5, i.e., the critical value at which the splash limits the saltation in the model of *Berzi et al.* [2016]. In that case, the minimum Shields parameter for continuing saltation is still given by equation (1), with equations (2) and (5), in which v_c is taken equal to 5.

Using equations (2) and (5) in equation (1), with the take-off velocity given by equation (8) provides the critical Shields parameter at infinite R,

$$S_c^{\infty} = \frac{K\kappa^2 \left[\ln\left(\frac{15\nu}{k_s u_c} \right) \right]^{-2} \left[\frac{A+D}{2} \frac{\nu}{u_c} + \left(\frac{A-D}{0.6} \right)^{1/2} \sigma^{1/2} \right]^2}{\sigma} \tag{9}$$

2.2 Effects of finite particle inertia

To determine the continuing saltation threshold at finite values of the particle Reynolds number, we first assume that the critical take-off velocity is still given by equation (8), independent of R, even when R is not large, and that the vertical drag can still be neglected. The validity of these strong assumptions will be assessed in the next section, where comparisons with the numerical solutions of the periodic trajectories are shown. Then, we have to consider four effects that become important at finite values of R and affect the expression of the horizontal fluid velocity, the roughness length and the critical Shields parameter.

First, is the influence of lubrication forces on the impact of the particle at the bed. Inverting equation (A13), with $v_i = -v_f = v_c$, gives

$$e_y = \frac{v_c \sigma \mathrm{R} + 62}{v_c \sigma \mathrm{R} - 62}, \tag{10}$$

while, from equations (A14) and (A15),

$$e = a - b \frac{a_y}{e_y + b_y}. \tag{11}$$

The coefficients of restitution are now functions of the density ratio and the particle Reynolds number. From equation (A15),

$$u_f = \frac{e_y + b_y}{a_y} v\,, \tag{12}$$

and, from equation (A12),

$$u_i^2 = \left[e\left(u_f^2 + v_c^2 \right)^{1/2} - \frac{62(1+e)}{\sigma \mathrm{R}} \right]^2 - v_c^2. \tag{13}$$

Second, is the influence of both form and viscous drag in the horizontal momentum balance for the particle. In this case, the horizontal depth-averaged fluid velocity is given by the quadratic (see Appendix B)

$$\bar{U}^2 + \left(\frac{18}{0.3\mathrm{R}} - u_i - u_f \right) \bar{U} + u_i u_f - \frac{18}{0.3\mathrm{R}} \frac{u_i - u_f \exp\left[36\nu_c / (\sigma \mathrm{R}) \right]}{1 - \exp\left[36\nu_c / (\sigma \mathrm{R}) \right]} = 0, \tag{14}$$

where we have employed the ballistic time of flight, $t_f = 2v_c$.

Third, is the nature of the bed and the corresponding value of the roughness length. At finite values of R, the bed can be hydrodynamically smooth, transitional or rough, depending on the ratio between the roughness length and the thickness of the viscous sublayer [*Schlichting and Gersten*, 2000]. The critical Shields number, S_c, for having continuing saltation is, then, from equations (1) and (2), the implicit solution of:

$$S_c = K\kappa^2 U^2 \left[\ln\left(\frac{v_c^2}{2y_0}\right)\right]^{-2}, \tag{15}$$

where U is given by equation (14), with equations (8) and (10)-(13), and the roughness length is, for instance [*Guo and Julien*, 2007],

$$y_0 = \frac{1}{9\mathrm{R}^*} + \frac{k_s}{30}\left\{1-\exp\left[-\frac{k_s \mathrm{R}^*}{26}\right]\right\}, \tag{16}$$

where $\mathrm{R}^* = \mathrm{R}\left(\sigma S_c\right)^{1/2}$ is the boundary Reynolds number based on shear velocity. When R^* is less than 5 or greater than 70, the bed is hydrodynamically smooth or rough, respectively [*Schlichting and Gersten*, 2000]; for intermediate values, the bed is transitional.
Equation (15), with equation (16), can be solved via a successive substitution scheme or a Newton-Raphson method, using, as a first guess, the threshold value of the Shields parameter obtained from equation (15) with $y_0 = k_s/30$ – the rough limit. Alternatively, the limit of large R can be dealt with as above; and, in the limit of small R, where $y_0 \doteq 1/(9\mathrm{R}^*)$, R^* expanded as a quadratic in $\ln \mathrm{R}^*$ about $\ln \mathrm{R}^* = 1/10$, leading to a cubic equation for $\ln \mathrm{R}^*$. For values of $\ln \mathrm{R}^*$ less than unity, the solution of the cubic provides an approximate expression for $\ln \mathrm{R}^*$ and, therefore, for S_c (see Appendix C for more details).

Fourth, is the inter-particle cohesion, which becomes important at small values of R. There are several factors responsible for inter-particle cohesion. If we disregard the possibility of chemical binding, cohesion is caused by the combined effects of van der Waals forces, electrostatics, and liquid bridges. The most sophisticated approach would be to take into account the role of cohesive forces in the collision of the particles with the bed, and to modify the coefficients of restitution accordingly [*Brilliantov et al.*, 2007; *Luding*, 2008; *Pasha et al.*, 2014]. Here, we prefer to adopt a simpler approach by incorporating a yield value for the particle shear stress associated with a Coulomb cohesion term, χ [*Richefeu et al.*, 2006]. Then, the minimum Shields parameter for continuing saltation in the presence of cohesion, S_c^*, must exceed the threshold in absence of cohesion, S_c, by a quantity equal to χ:

$$S_c^* = S_c + \chi. \tag{17}$$

It has been shown that van der Waals and electrostatic forces [*Shao and Lu*, 2000], and the force associated with the presence of liquid bridges [*Richefeu et al.*, 2006] are all proportional to the particle diameter. Hence (see Appendix D), equation (17) becomes

$$S_c^* = S_c + \frac{\mathrm{B_n}}{\sigma \mathrm{R}} \tag{18}$$

where $\mathrm{B_n} = \gamma / \left[\mu_f \sqrt{gd(\sigma-1)/\sigma}\right]$ is a Bingham number and γ is the dimensional specific inter-particle force (in N/m). When cohesion is due to van der Waals and electrostatic forces, γ is of order 10^{-5} N/m [*Shao and Lu*, 2000]; when cohesion is due to liquid bridges, γ is of order 10^{-1} N/m [*Richefeu et al.*, 2006].

3 Discussion and comparisons

We first test the capability of the present theory to reproduce the results obtained by numerically solving the differential equations governing the periodic trajectories given in

Appendix A. The process of obtaining the saltation threshold from the numerical solutions to the periodic trajectories is tedious. We initially fix the values of the density ratio and particle Reynolds number; then, we compute the periodic trajectory in the limit of vanishing vertical mass flux for successive decreasing values of the Shields parameter, using the "bvp4c" solver in MATLAB, until we reach a point where no steady solution exists. The smallest value of the Shields parameter compatible with the existence of a steady solution is taken to be the threshold.. It is worth emphasizing that the numerical solutions to the periodic trajectories do not include the effect of inter-particle cohesion. Figure 2 shows that the solution of equation (15), with equations (8), (10)-(13) and (16), is in excellent agreement with the results of the numerical solutions to the periodic trajectories for all values of σ and R. The solution also permits an easy check on the influence of finite particle inertia mentioned in the previous Section. We can ignore the influence of the lubrication forces on the impact with the bed by using equations (3) and (4) instead of equations (12) and (13) in equation (14); and we can consider the bed as always hydrodynamically rough by using $y_0 = k_s / 30$ instead of equation (16).

At small density ratios (e.g., σ = 2.5), the bed is always hydrodynamically rough (the values of R^* for the all the data considered here are reported in Figure 3; for the same density ratio, different values of R^* indicate that particles of different size have been employed) and the lubrication forces during the impact with the bed are responsible for the decrease of S_c with R. At large density ratios (e.g., σ = 2500), the effect of lubrication forces is always negligible, but the hydrodynamic nature of the bed has a strong influence on the saltation threshold. For intermediate values of the density ratio both effects are important.

We next make comparisons with the results of discrete element simulations of spheres coupled with a continuum. Reynolds-averaged description of the fluid hydrodynamics in a quasi-2D domain [*Durán et al.*, 2012]. The density ratio was changed in the range comprised between 2 and 2000, while the product $R\sigma^{1/2}$ was kept constant and equal to ten; consequently, the bed was hydrodynamically smooth (Figure 3). In the simulations, both the non-linear drag, and the presence of a viscous sublayer were modelled; while neither the influence of lubrication forces on particle collisions nor inter-particle cohesion were included. The measured threshold should, therefore, be compared with the solution of equation (15), together with equations (8) and (16), in which the fluid depth-averaged velocity is given by equation (14), with equations (3) and (4). Figure 4 shows a reasonable agreement between the present theory, which correctly capture the decrease of the threshold with the density ratio, and the results of the simulations.

Iversen and White [1982] proposed an expression for the static threshold of saltation in the absence of cohesive forces of the type $S_c = S_c\left(R^*\right)$, where the dependence on R^* must be determined by fitting to experimental data. *Shao and Lu* [2000] further simplified the expression of *Iversen and White* and proposed that $S_c = 0.0123$. If the product $R\sigma^{1/2}$ is kept constant, neither model is able to capture the density ratio dependence shown in Figure 4. *Iversen et al.* [1987] suggested a modification to the expression of *Iversen and White* [1982] that includes a dependence on the density ratio to be once again determined by fitting with experiments. Unfortunately, *Iversen et al.* [1987] were only able to provide an explicit expression for R^* larger than 10. *Lu et al.* [2005] were able to include non-empirically a dependence of the static threshold on the density ratio through the role of the turbulent fluctuations. Given that turbulent fluctuations are not present in the numerical simulations of *Durán et al.* [2012], that model cannot explain the results shown in Figure 4.

Unlike these examples, models of the dynamic threshold naturally include a dependence on the density ratio. The two-species model of *Andreotti* [2004] has been developed in the limit of large particle Reynolds number, and therefore does not apply to the conditions of *Durán et al.* [2012]. As already mentioned, it has been extended to small values of R by *Claudin and Andreotti* [2006], but the threshold must be obtained via numerical integration of differential equations. The predictions of the explicit model of *Pähtz et al.* [2012] are in excellent agreement with the numerical simulations for large density ratio, but strongly overpredict the threshold for σ less than 100 (Figure 4). The model of *Pähtz and Durán* [2016] is in better agreement with the data for small density ratios. It is worth emphasizing that our approach permits the dependence on the dimensionless numbers governing the phenomenon to be expressed explicitly.

Finally, we make comparisons with available experiments performed in wind tunnels [*Iversen and White*, 1982; *Burr et al.*, 2015]. In these experiments, the density ratio was kept constant, while the size of the particles was changed, thus changing the particle Reynolds number. Actually, changing the size of the particles has an effect also on the Bingham number, and this must be taken into account to correctly evaluate the role of cohesive forces. Given the fluid properties and the gravitational acceleration in the experiments, the Bingham number can be simply related to the particle Reynolds number: $B_n \propto R^{-1/3}$ (see Appendix D).

In the experiments performed by *Burr et al.* [2015], the threshold was identified as the value of the Shields parameter (actually, the fluid shear velocity) at which there was a continuous motion over 50% of the central region around the longitudinal axis of the bed. This criterion is certainly arbitrary, but, in the absence of more rigorous measurements, we make comparisons with those data that are, at least, consistent with our picture of continuing saltation. In the experiments performed by *Iversen and White* [1982] at $\sigma = 2083$, the measured threshold is also consistent with the continuing saltation threshold. Experiments for $\sigma = 40$ are also available [*Greeley et al.*, 1984], but the experimental criterion to determine the threshold, based on the beginning of sporadic saltation of groups of grains, has more to do with intermittent motion than with continuing saltation. Consistently, our theory (not shown here for brevity) overpredicts the experimental threshold in that case. Figure 5 shows that the present theory is able to reproduce the experimental points at low values of the particle Reynolds number only if the effect of cohesion (equation 18) is included. To match the experiments, we use $K = 1$ (to fit the few points in the high R limit when $\sigma = 76$), and $B_n = 10R^{-1/3}$, independent of the density ratio. This corresponds to values of γ close to 10^{-5} N/m, indicating that van der Waals and electrostatic forces are the sources of cohesion (Appendix D).

Here, it seems worthwhile to review the coefficients, other than the fluid and particle properties, that enter our theory in absence of cohesion. This indicates how the predictions of the model might be refined.

In our theory, the four coefficients a, b, a_y and b_y (of which only 3 are actually independent) in the expressions for the coefficients of restitution (equations A14 and A15) can be, in principle, determined for any types of particle and bed from experiments or simulations [*Beladjine et al.*, 2007]. The dependence of the coefficients of restitution on the product σR (equations A12 and A13) has been taken from the theoretical analysis of lubrication by *Barnocky and Davis* [1988]. This dependence can be refined from ad hoc

experiments on the impact of two particles immersed in a viscous fluid at different relative colliding velocities [*Gondret et al.*, 2002; *Yang and Hunt*, 2006].

We use an expression for the steady fluid drag exerted on the particle that is valid for spheres (equation A1). Other particles (such as the walnut shells used by *Burr et al.* [2015]) and the incorporation of unsteady effects might require a different expression.

The value of the roughness k_s can be determined from measurements of the origin of the logarithmic fluid velocity profile, such as those performed – but unfortunately not reported – by *Burr et al.* [2015]. In water, k_s has been estimated to be about 2.5 particle diameters [*van Rijn*, 1984], rather than one diameter as adopted here. The effect of changing k_s from 1 to 2.5 is shown in Figure 6, where the Shields parameter at the saltation threshold is plotted versus the particle Reynolds number when $\sigma = 76$ and cohesion is neglected.

The parameter K in the expression of the fluid shear stress at the bed (equation 1) must be introduced because of the approximate integration of the logarithmic fluid velocity profile over the trajectory height [*Berzi et al.*, 2016] and the assumption that the fluid velocity is uniform when solving the horizontal particle momentum balance. Consequently, K is the only fitting parameter for cohesionless particles in our model for the continuing saltation threshold, although we do know that it must be of order unity. The effect of changing K from 1.5 to 1 when $\sigma = 76$ is also depicted in Figure 6. Actually, K can be fit from measurements of the saltation threshold at large particle Reynolds number, where S_c saturates.

4 Conclusions

We have developed a method to predict the threshold for continuing saltation in a turbulent shearing flow that is valid at arbitrary values of the particle-to-fluid density ratio and fall particle Reynolds number. Consequently, the predictions apply to both terrestrial and extra-terrestrial conditions. The treatment is based on analytical solutions for periodic trajectories – those endless, identical, jumps that a single particle must follow in steady motion. If all of the particles in the system are imagined to follow such a periodic trajectory, there is a minimum shear stress that the fluid must exert at the bed to sustain the motion. We have identified this with the threshold for continuing saltation.

We have shown how viscous and form drag, lubrication forces, the hydrodynamic nature of the bed, and cohesive forces influence this threshold. The expression for the threshold permits the isolation of individual physical mechanisms and allows their contribution to be quantified. At large density ratios, as in Aeolian saltation on Earth or Mars, the lubrication forces are negligible. The bed can be hydrodynamically smooth, transitional or rough and the decrease in the Shields parameter with the increase in the fall particle Reynolds number is due to cohesion. At small density ratios, as in aquatic saltation on Earth, the lubrication forces are effective in damping the impact of the particles with the bed, the fluid force is due to a combination of viscous and form drag, and the bed is, typically, hydrodynamically rough. At large values of the fall particle Reynolds number, there is a dependence of the Shields parameter on the density ratio, not accounted for in previous formulations, due to form drag. At small values of the fall particle Reynolds number, inter-particle cohesion is dominant.

We have shown that the present theory is capable of reproducing the quantitative determinations of thresholds made in discrete element simulations of spheres, coupled with a Reynolds-averaged description of the fluid, and the physical experiments in wind tunnels, meant to reproduce Aeolian saltation on Earth and Titan.

We have characterized the strength of the minimum fluid shear stress at the bed for which continuing saltation is possible and indicated how this threshold depends upon the properties of the fluid and the particles. Consequently, evidence of particle flows in the geologic record or in observations of distant bodies provides lower bounds on fluid velocities and, perhaps, information regarding the nature of the particles on the surface of a distant body.

Appendix A: Numerical solutions of the periodic trajectories

We briefly summarize the equations that govern the periodic saltation. If the flow is steady and uniform, the velocities are only functions of the vertical distance from the bed *y*. We characterize the drag exerted on the particles through a nonlinear drag coefficient, which is, in dimensionless form,

$$C_D = \frac{0.3}{\sigma}\sqrt{(U-u)^2+v^2} + \frac{18}{\sigma \mathrm{R}}, \tag{A1}$$

In the following, we use the subscripts plus and minus to label quantities in the upward and downward parts of a trajectory, respectively. The upward and downward components of the particle velocity are governed by

$$v^+ \frac{\mathrm{d}u_+}{\mathrm{d}y} = C_D^+ \left(U - u^+\right), \tag{A2}$$

$$v^+ \frac{\mathrm{d}v^+}{\mathrm{d}y} = -1 - C_{D^+} v^+, \tag{A3}$$

and

$$v^- \frac{\mathrm{d}u^-}{\mathrm{d}y} = C_{D^-} \left(U - u^- \right), \tag{A4}$$

$$v^- \frac{\mathrm{d}v^-}{\mathrm{d}y} = -1 - C_{D^-} v^-, \tag{A5}$$

respectively. The horizontal coordinates x^+ and x^- are functions of the vertical coordinate y,

$$v^+ \frac{\mathrm{d}x^+}{\mathrm{d}y} = u^+, \tag{A6}$$

and

$$v^- \frac{\mathrm{d}x^-}{\mathrm{d}y} = u^-. \tag{A7}$$

Upon employing Prandtl's mixing length hypothesis, the horizontal velocity of the turbulent fluid is given in terms of fluid shear stress S by

$$\frac{\mathrm{d}U}{\mathrm{d}y} = \frac{\left(\sigma S \right)^{1/2}}{\kappa \left(y + y_0 \right)}, \tag{A8}$$

where $\kappa = 0.41$ is von Kármán's constant and y_0 is the dimensionless roughness length. An expression for the latter, valid for hydrodynamically smooth, rough and transitional beds, is [*Guo and Julien*, 2007]

$$y_0 = \frac{1}{9 \mathrm{R} \left(\sigma S \right)^{1/2}} + \frac{k_s}{30} \left\{ 1 - \exp\left[-\frac{\left(\sigma \mathrm{R} S \right)^{1/2}}{26} \right] \right\}, \tag{A9}$$

where k_s is the roughness, here taken to be equal to one particle diameter [*Jenkins and Valance*, 2014].

The fluid shear stress, S, is the difference between the dimensionless fluid shear stress far from the bed, S^* - the Shields parameter – and the particle shear stress s: $S = S^* - s$. The particle shear stress is

$$s \equiv -\left(c^+ v^+ u^+ + c^- v^- u^- \right), \tag{A10}$$

where c is the particle concentration. In steady, uniform saltation, the vertical mass fluxes of ascending and descending particles must balance at any point, and must be independent of the vertical position. Hence,

$$c^+ v^+ = -c^- v^- = \phi_0, \tag{A11}$$

where ϕ_0 is the vertical mass flux at the bed, i.e., the pick-up function.

The system of equations A1 through A11 permits the determination of the seven unknowns u^+, v^+, u^-, v^-, x^+, x^-, and U, after the application of seven boundary conditions. The latter are the kinematic relations $x^+(0) = 0$, $x^-(0) = L$, $x^+(H) = x^-(H)$, $u^+(H) = u^-(H)$, $v^+(H) = v^-(H) = 0$, where H and L are the height and the length of the periodic particle

trajectory, and the no-slip condition $U(0)=0$. The trajectory height and length can be determined as part of the solution, given the two conditions for the periodic rebound of a particle at the bed:

$$\left(u_i^2+v_i^2\right)^{1/2}=e\left(u_f^2+v_f^2\right)^{1/2}-\frac{62(1+e)}{\sigma \mathrm{R}}, \tag{A12}$$

where $u_i=u^+(0)$, $u_f=u^-(0)$, $v_i=v^+(0)$, and $v_f=v^-(0)$; and

$$v_i=-e_y v_f-\frac{62\left(1+e_y\right)}{\sigma \mathrm{R}}, \tag{A13}$$

where e and e_y are determined in terms of the parameters a, b, a_y and b_y and the tangent of the angle of departure v_f/u_f measured in the collision experiments [*Beladjine et al.*, 2007] by

$$e\equiv a+b\frac{v_f}{u_f}, \tag{A14}$$

and

$$e_y\equiv -a_y\frac{u_f}{v_f}-b_y. \tag{A15}$$

The parameters a, b, a_y and b_y are numerical constants that depend on the coefficients of normal restitution and sliding friction of the particles and whether the bed is rigid or erodible [*Oger et al.*, 2005; *Beladjine et al.*, 2007; *Crassous et al.*, 2007]. In equations (A12) and (A13), we assume that the coefficients of restitution in a rebound depend on the product of the density ratio and the fall particle Reynolds number in the same way as the coefficient of normal restitution in a binary collision derived by *Barnocky and Davis* [1988] and experimentally confirmed [*Gondret et al.*, 2002; *Yang and Hunt*, 2006].

The numerical solution to the periodic trajectory is determined by two inputs: the Shields parameter, S^*, and the pick-up function ϕ_0, or, equivalently, the vertical velocity after the rebound, v_i.

Appendix B: Integration of the particle horizontal momentum balance

If we assume that the fluid horizontal velocity is uniform and equal to $\bar{U}$, with the drag coefficient given by equation (A1) and neglect the particle vertical velocity there, the horizontal momentum balance for the particle is,

$$\frac{\mathrm{d}u}{\mathrm{d}t}=\frac{0.3}{\sigma}\left(\bar{U}-u\right)^2+\frac{18}{\sigma \mathrm{R}}\left(\bar{U}-u\right). \tag{B1}$$

Integrating along the particle trajectory between $t = 0$, when $u = u_i$, and $t = t_f$ (time of flight), when $u = u_f$, gives

$$\frac{\bar{U}-u_i}{\bar{U}-u_f}\frac{0.3\left(\bar{U}-u_f\right)+18/\mathrm{R}}{0.3\left(\bar{U}-u_i\right)+18/\mathrm{R}}=\exp\left(\frac{18}{\sigma \mathrm{R}}t_f\right). \tag{B2}$$

At very large R, the viscous drag can be ignored in equation (B1), and the integration gives, approximately,

$$\bar{U} = \frac{u_f + u_i}{2} + \frac{1}{2}\left[\left(u_f - u_i\right)^2 + 4\left(\frac{u_f - u_i}{0.3t_f}\right)^2\sigma\right]^{1/2} \approx \frac{u_f + u_i}{2} + \left(\frac{u_f - u_i}{0.3t_f}\right)\sigma^{1/2} \tag{B3}$$

Appendix C: Critical Shields parameter in the limit of small particle inertia

Equation (15) can be written, with $y_0 = 1/(9\mathrm{R}^*)$ and $\mathrm{R}^* = (\sigma S_c)^{1/2}$, as

$$\mathrm{R}^*\left[\ln\left(\frac{9}{2}\nu_c^2\right) + \ln \mathrm{R}^*\right] = K^{1/2}\kappa U. \tag{C1}$$

Expanding R^* in powers of $\ln \mathrm{R}^*$ about $\ln \mathrm{R}^* = 1/10$ gives

$$\mathrm{R}^* = e^{1/10}\left[1 + \ln \mathrm{R}^* - \frac{1}{10} + \frac{1}{2}\left(\ln \mathrm{R}^* - \frac{1}{10}\right)^2\right]. \tag{C2}$$

Then, upon inserting equation (C2) into equation (C1),

$$e^{1/10}\left[\frac{1}{2}\left(\ln \mathrm{R}^*\right)^2 + \frac{9}{10}\ln \mathrm{R}^* + \frac{181}{200}\right]\left[\ln\left(\frac{9}{2}\nu_c^2\right) + \ln \mathrm{R}^*\right] = K^{1/2}\kappa U. \tag{C3}$$

Appendix D: Dimensionless cohesion

Coulomb cohesion is proportional to the tensile strength [*Richefeu et al.*, 2006] – the inter-particle force per unit area. If the dimensional inter-particle force is proportional to the particle diameter, then, in dimensionless terms, the Coulomb cohesion results

$$\chi = \frac{\gamma d}{\rho^s g(\sigma - 1)d^3/\sigma} = \frac{\gamma}{\mu^f\sqrt{g(\sigma-1)d/\sigma}}\frac{1}{\sigma \mathrm{R}} = \frac{\mathrm{B_n}}{\sigma \mathrm{R}}, \tag{D1}$$

where γ has the dimensions of N/m (effective surface tension), and $\mathrm{B_n}$ is a Bingham number – the ratio of cohesive to viscous forces.

In experiments, the properties of the fluid are usually kept constant, while the particle diameter is changed; hence, changing both the particle Reynolds number and the Bingham number. Inverting the relation between R and the particle diameter, and using it in the expression for $\mathrm{B_n}$ gives

$$\mathrm{B_n} = \frac{\gamma}{\mu^f\sqrt{g(\sigma-1)d/\sigma}} = \frac{\left(\rho^f\right)^{1/3}\gamma^{1/3}}{\left(\mu^f\right)^{4/3}\left[g(\sigma-1)/\sigma\right]^{1/3}}\frac{1}{\mathrm{R}}. \tag{D2}$$

In the experiments of *Burr et al.* [2015], $\rho^f = 14.5\,\mathrm{Kg/m^3}$, $\mu^f = 0.0000185\,\mathrm{Pa\cdot s}$ and $g = 9.806\,\mathrm{m/s^2}$; in the experiments of *Iversen and White* [1982], $\rho^f = 1.2\,\mathrm{Kg/m^3}$, $\mu^f = 0.00001\,\mathrm{Pa\cdot s}$ and $g = 9.806\,\mathrm{m/s^2}$. Using these in equation (D2) gives, , with γ of order 10^{-5} N/m, approximately

$$\mathrm{B_n} \approx \frac{10}{\mathrm{R}^{1/3}}. \tag{D3}$$

A more refined approach to cohesion has been proposed by *Claudin and Andreotti*

[2006], whose analysis indicates that $\gamma = \gamma_a \left(\rho^s g d / E \right)^{1/3}$, where γ_a is the actual surface

tension and E the Young modulus of the particles. However, this additional slight dependence of γ on the particle diameter cannot be discerned, given the experimental scattering.

Acknowledgements. All data for this paper are properly cited and referred to in the reference list. We are grateful to the referees for constructive comments that led to improvements in the manuscript.

References

Abbott, J. E., and J. R. D. Francis (1977), Saltation and suspension trajectories of solid grains in a water stream, *Philos. Trans. R. Soc. A Math. Phys. Eng. Sci.*, *284*(1321), 225–254, doi:10.1098/rsta.1977.0009.

Ancey, C., F. Bigillon, P. Frey, J. Lanier, and R. Ducret (2002), Saltating motion of a bead in a rapid water stream, *Phys. Rev. E*, *66*(3), 036306, doi:10.1103/PhysRevE.66.036306.

Andreotti, B. (2004), A two-species model of aeolian sand transport, *J. Fluid Mech.*, *510*, 47–70, doi:10.1017/S0022112004009073.

Bagnold, R. A. (1941), *The Physics of blown sand and desert dunes*, Methuen, New York.

Barnocky, G., and R. H. Davis (1988), Elastohydrodynamic collision and rebound of spheres: Experimental verification, *Phys. Fluids*, *31*, 1324–1329, doi:10.1063/1.866725.

Beladjine, D., M. Ammi, L. Oger, and A. Valance (2007), Collision process between an incident bead and a three-dimensional granular packing, *Phys. Rev. E*, *75*(6), 061305, doi:10.1103/PhysRevE.75.061305.

Berzi, D., J. T. Jenkins, and A. Valance (2016), Periodic saltation over hydrodynamically rough beds: aeolian to aquatic, *J. Fluid Mech.*, *786*, 190–209, doi:10.1017/jfm.2015.601.

Brilliantov, N. V., N. Albers, F. Spahn, and T. Poschel (2007), Collision dynamics of granular particles with adhesion, *Phys. Rev. E*, *76*(5), 1–12, doi:10.1103/PhysRevE.76.051302.

Burr, D. M., N. T. Bridges, J. R. Marshall, J. K. Smith, B. R. White, and J. P. Emery (2015), Higher-than-predicted saltation threshold wind speeds on Titan, *Nature*, *517*, 60–63, doi:10.1038/nature14088.

Charru, F., B. Andreotti, and P. Claudin (2013), Sand ripples and dunes, *Annu. Rev. Fluid Mech.*, *45*(1), 469–493, doi:10.1146/annurev-fluid-011212-140806.

Claudin, P., and B. Andreotti (2006), A scaling law for aeolian dunes on Mars, Venus, Earth, and for subaqueous ripples, *Earth Planet. Sci. Lett.*, *252*, 30–44, doi:10.1016/j.epsl.2006.09.004.

Crassous, J., D. Beladjine, and A. Valance (2007), Impact of a projectile on a granular medium described by a collision model, *Phys. Rev. Lett.*, *99*(24), 248001, doi:10.1103/PhysRevLett.99.248001.

Drake, T. G., R. L. Shreve, W. E. Dietrich, P. J. Whiting, and L. B. Leopold (1988), Bedload transport of fine gravel observed by motion-picture photography, *J. Fluid Mech.*, *192*, 193, doi:10.1017/S0022112088001831.

Durán, O., B. Andreotti, and P. Claudin (2012), Numerical simulation of turbulent sediment transport, from bed load to saltation, *Phys. Fluids*, *24*, 103306, doi:10.1063/1.4757662.

Fernandez Luque, R., and R. Van Beek (1976), Erosion and transport of bed-load sediment, *J. Hydraul. Res.*, *14*(2), 127–144, doi:10.1080/00221687609499677.

Gao, P. (2008), Transition between two bed-load transport regimes: saltation and sheet flow, *J. Hydraul. Eng.*, *134*, 340–349, doi: 10.1061/(ASCE)0733-9429(2008)134:3(340).

Gondret, P., M. Lance, and L. Petit (2002), Bouncing motion of spherical particles in fluids, *Phys. Fluids*, *14*(2), 643, doi:10.1063/1.1427920.

Greeley, R., J. Iversen, R. Leach, J. Marshall, S. Williams, and B. White (1984), Windblown sand on Venus - Preliminary results of laboratory simulations, *Icarus*, *57*, 112–124, doi:10.1016/0019-1035(84)90013-7.

Guo, J., and P. Y. Julien (2007), Buffer law and transitional roughness effect in turbulent open-channel flows, in *The Fifth International Symposium on Environmental Hydraulics* (ISEH V), pp. 1–6.

Hansen, C. J., A. S. McEwen, A. P. Ingersoll, and R. J. Terrile (1990), Surface and airborne evidence for plumes and winds on triton, *Science* 250, 421–424.

Iversen, J., R. Greeley, J. R. Marshall, and J. B. Pollack (1987), Aeolian saltation threshold: the effect of density ratio, *Sedimentology*, *34*, 699–706, doi:10.1111/j.1365-3091.1987.tb00795.x.

Iversen, J. D., and B. R. White (1982), Saltation threshold on Earth, Mars and Venus, *Sedimentology*, *29*, 111–119, doi:10.1111/j.1365-3091.1982.tb01713.x.

Iversen, J. D., J. B. Pollack, R. Greeley, and B. R. White (1976), Saltation threshold on Mars: The effect of interparticle force, surface roughness, and low atmospheric density, *Icarus*, *29*(3), 381–393, doi:10.1016/0019-1035(76)90140-8.

Jenkins, J. T., I. Cantat, and A. Valance (2010), Continuum model for steady, fully developed saltation above a horizontal particle bed, *Phys. Rev. E*, *82*, 020301, doi:10.1103/PhysRevE.82.020301.

Jenkins, J. T., and A. Valance (2014), Periodic trajectories in aeolian sand transport, *Phys. Fluids*, *26*(7), 073301, doi:10.1063/1.4885576.

Kok, J. F. (2010), An improved parameterization of wind-blown sand flux on Mars that includes the effect of hysteresis, *Geophys. Res. Lett.*, *37*(12), 1–6, doi:10.1029/2010GL043646.

Kok, J. F., E. J. R. Parteli, T. I. Michaels, and D. B. Karam (2012), The physics of wind-blown sand and dust, *Rep. Prog. Phys.*, *75*(10), 106901, doi:10.1088/0034-4885/75/10/106901.

Lajeunesse, E., L. Malverti, and F. Charru (2010), Bed load transport in turbulent flow at the grain scale: Experiments and modeling, *J. Geophys. Res. Earth Surf.*, *115*, F04001, doi:10.1029/2009JF001628.

Lorenz, R. D. et al. (2006), The sand seas of Titan: Cassini RADAR observations of longitudinal dunes., *Science*, *312*(5774), 724–727, doi:10.1126/science.1123257.

Lu, H., M. R. Raupach, and K. S. Richards (2005), Modeling entrainment of sedimentary particles by wind and water: A generalized approach, *J. Geophys. Res. Atmos.*, *110*(24), 1–17, doi:10.1029/2005JD006418.

Luding, S. (2008), Cohesive, frictional powders: Contact models for tension, *Granul. Matter*, *10*(4), 235–246, doi:10.1007/s10035-008-0099-x.

Maurin, R., J. Chauchat, B. Chareyre, and P. Frey (2015), A minimal coupled fluid-discrete element model for bedload transport, *Phys. Fluids*, 27(11), 113302, doi:10.1063/1.4935703.

Maxey, M. R., and J. J. Riley (1983), Equation of motion for a small rigid sphere in a nonuniform flow, *Phys. Fluids*, *26*(1983), 883, doi:10.1063/1.864230.

Nelson, J. M., R. L. Shreve, S. R. McLean, and T. G. Drake (1995), Role of near-bed turbulencein bed load transport and bed form mechanics, *Water Resour. Res.*, *31*(8), 2071–2086, doi:10.1029/95WR00976.

Niño, Y., and M. García (1998), Experiments on saltation of sand in water, *J. Hydraul. Eng.*, *124*(10), 1014–1025, doi:10.1061/(ASCE)0733-9429(1998)124:10(1014).

Oger, L., M. Ammi, A. Valance, and D. Beladjine (2005), Discrete Element Method studies of the collision of one rapid sphere on 2D and 3D packings., *Eur. Phys. J. E*, *17*(4), 467–76, doi:10.1140/epje/i2005-10022-x.

Pähtz, T., and O. Durán (2016), Unified threshold model suggests sand transport by wind on Triton, Pluto, and comet 67P, ArXiv ID: 1602.07079, 1–34.

Pähtz, T., J. F. Kok, and H. J. Herrmann (2012), The apparent roughness of a sand surface blown by wind from an analytical model of saltation, *New J. Phys.*, *14*, doi:10.1088/1367-2630/14/4/043035.

Pasha, M., S. Dogbe, C. Hare, A. Hassanpour, and M. Ghadiri (2014), A linear model of elasto-plastic and adhesive contact deformation, *Granul. Matter*, *16*(1), 151–162, doi:10.1007/s10035-013-0476-y.

Richefeu, V., M. S. El Youssoufi, and F. Radjaï (2006), Shear strength properties of wet granular materials, *Phys. Rev. E*, *73*(5), 1–11, doi:10.1103/PhysRevE.73.051304.

van Rijn, L. (1984), Sediment transport, part I: bed load transport, *J. Hydraul. Eng.*, *110*(10), 1431–1456, doi:10.1061/(ASCE)0733-9429(1984)110:10(1431).

Sagan, C., and C. Chyba (1990), Triton's streaks as windblown dust, *Nature*, 346, 546–548.

Sauermann, G., K. Kroy, and H. J. Herrmann (2001), A continuum saltation model for sand dunes, *Phys. Rev. E*, *64*, 031305, doi:10.1103/PhysRevE.64.031305.

Schlichting, H., and K. Gersten (2000), *Boundary-layer theory*, Springer, Berlin.

Schmeekle, M. W. (2014), Numerical simulation of turbulence and sediment transport of medium sand, *J. Geophys. Res.*, *119*, 1240–1262, doi:10.1002/2013JF002911.

Shao, Y., and H. Lu (2000), A simple expression for wind erosion threshold friction velocity, *J. Geophys. Res.*, *105*, 22437–22443, doi:10.1029/2000JD900304.

Thomas, N. et al. (2015), Redistribution of particles across the nucleus of comet 67p/Churyumov-Gerasimenko. *Astron. Astrophys.*, 583, A17, doi:10.1051/0004-6361/201526049.

Valance, A., K. R. Rasmussen, A. Ould, El Moctar, and P. Dupont (2015), The physics of Aeolian sand transport, *Compt. Rend. Phys.*, *16*(1), 105–117, doi:10.1016/j.crhy.2015.01.006.

Ward, B. D. (1969), Relative density effects on incipient bed movement, *Water Resour. Res.*, *5*(5), 1090–1096, doi:10.1029/WR005i005p01090.

Yang, F.-L., and M. L. Hunt (2006), Dynamics of particle-particle collisions in a viscous liquid, *Phys. Fluids*, *18*(12), 121506, doi:10.1063/1.2396925.

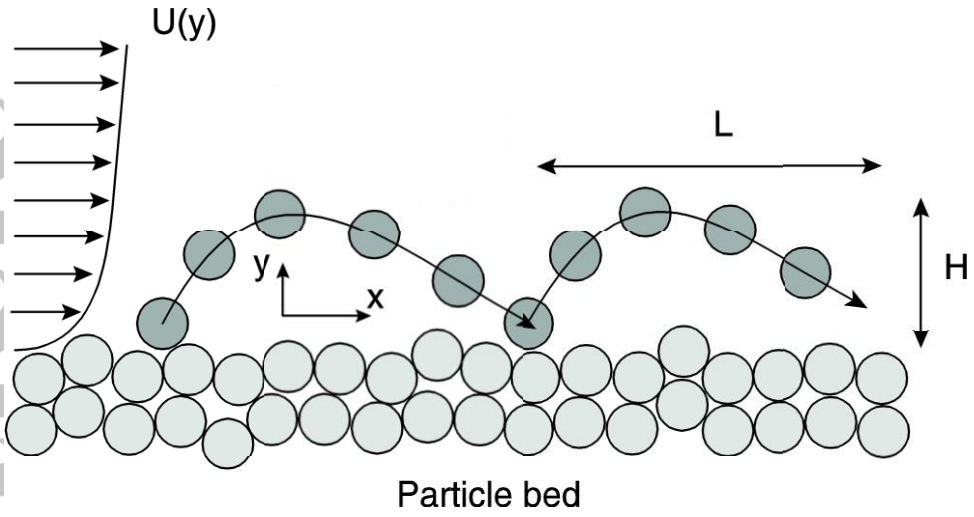

Figure 1. Sketch of the periodic trajectory: *L* and *H* are the trajectory length and height, respectively; *U* is the horizontal fluid velocity.

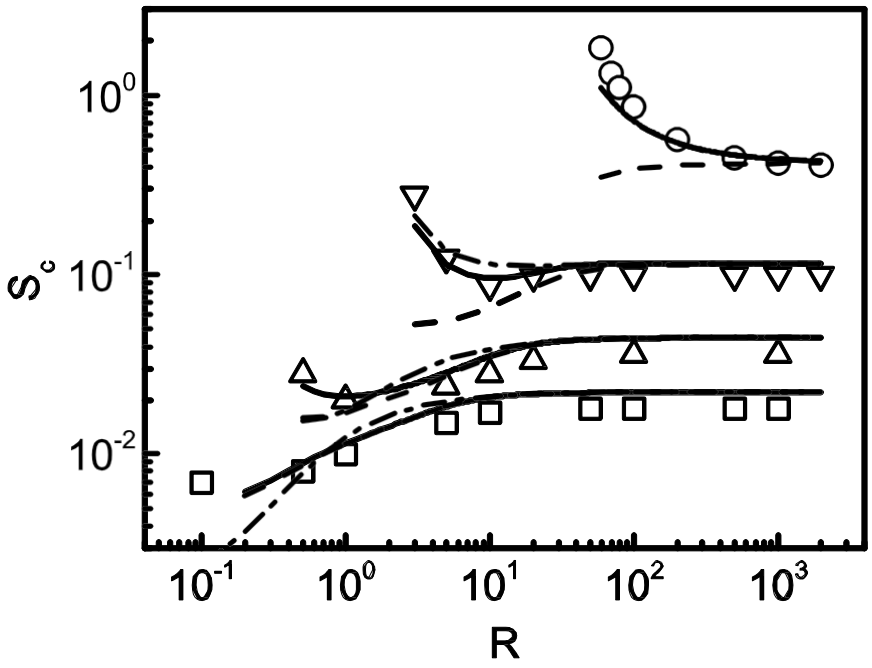

Figure 2. Numerical (symbols, from numerical solutions of the periodic trajectories) critical Shields parameter, S_c, for continuing saltation as a function of the particle Reynolds number, R, for particle-to-fluid density ratios: $\sigma = 2.5$ (circles), $\sigma = 25$ (lower triangles), $\sigma = 250$ (upper triangles) and $\sigma = 2500$ (squares). The solid lines represent the solution of equation (15) when both the lubrication forces and the hydrodynamic nature of the bed are included. The dashed and dot-dashed lines represent the solution when either lubrication forces are ignored or the bed is considered hydrodynamically rough, respectively.

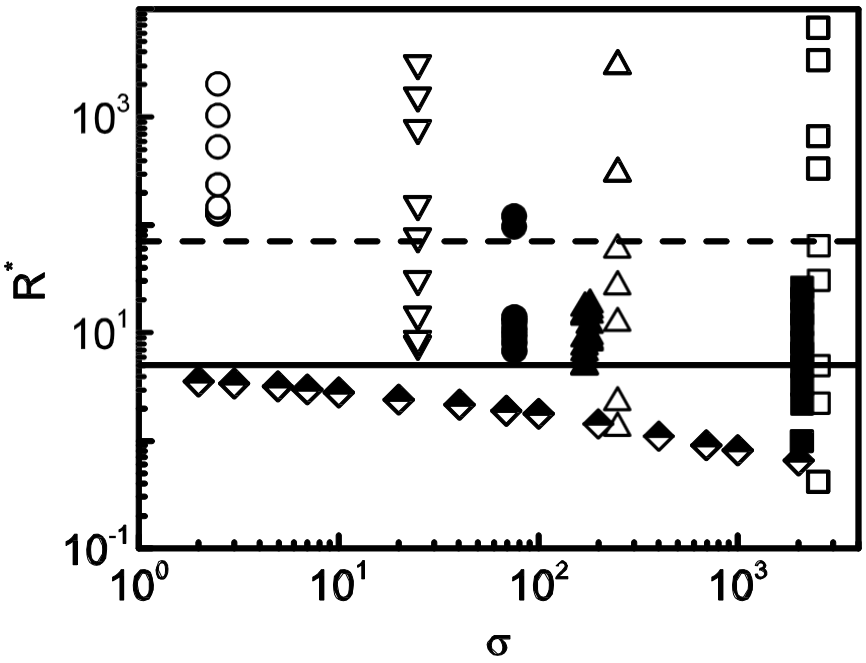

Figure 3. Boundary Reynolds number, R^*, at the saltation threshold as a function of the density ratio, σ, for data reported in previous investigations: numerical solutions of the periodic trajectories (open symbols, same as in Figure 2); discrete element simulations [*Durán et al.*, 2012] (half-filled diamonds); and experiments in wind tunnels [*Iversen and White*, 1982; *Burr et al.*, 2015] (filled symbols). Also shown are the upper and lower limits for hydrodynamically smooth (solid line) and rough (dashed line) beds.

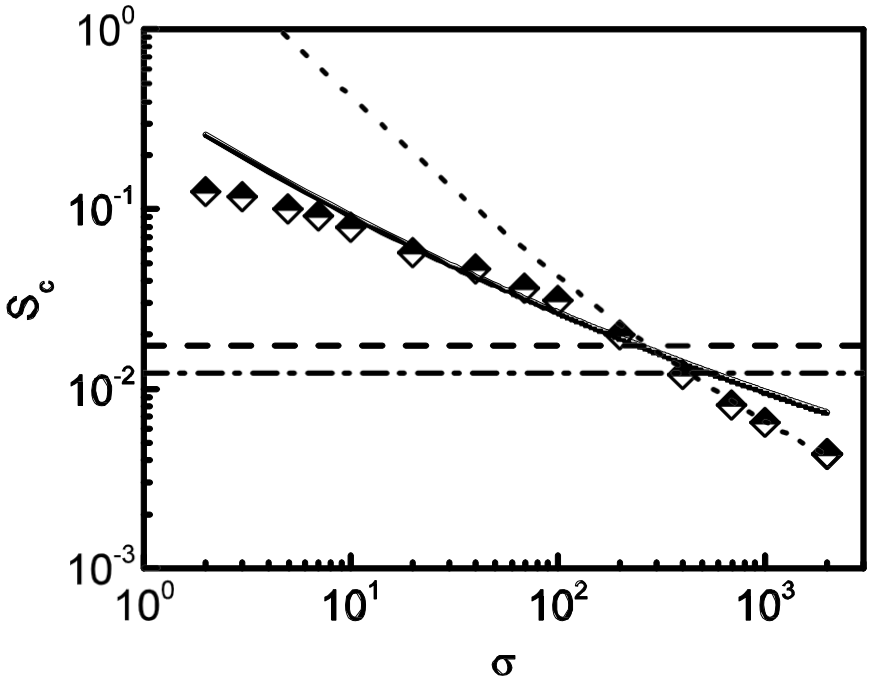

Figure 4. Critical Shields parameter, S_c, as a function of the density ratio, σ, when $R\sigma^{1/2}=10$: discrete element simulations [*Durán et al.*, 2012] (diamonds); present theory without lubrication forces and cohesion (solid line); *Iversen and White*'s model [1982] (dashed line); *Shao and Lu*'s model [2000] (dot-dashed line); *Pähtz et al.*'s model [2012] (dotted line).

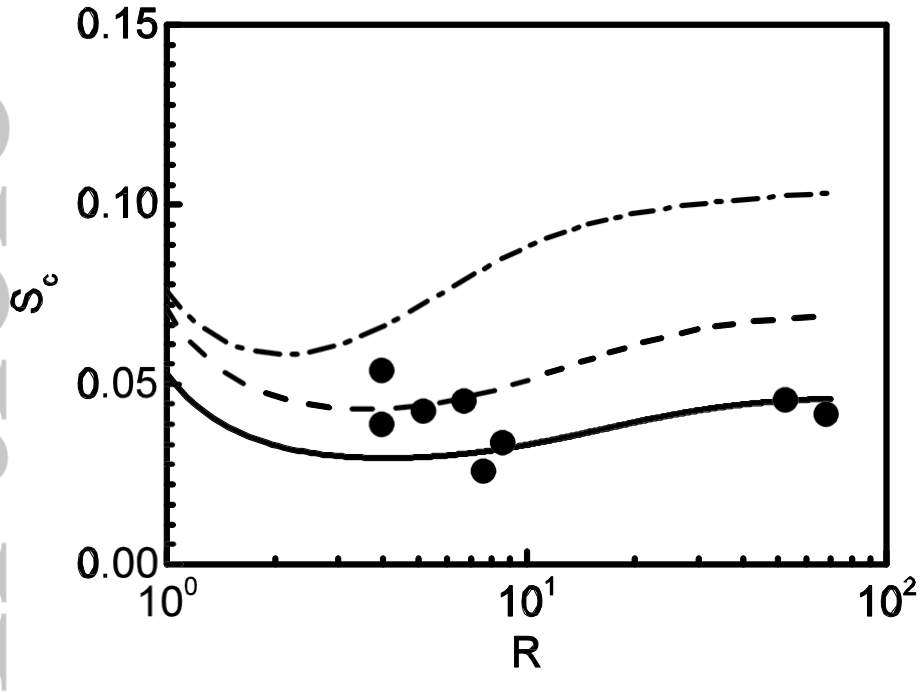

Figure 6. Theoretical (lines) critical Shields parameter, S_c, in the absence of cohesion as a function of the particle Reynolds number, R; for particle-to-fluid density ratio $\sigma = 76$ when: $K = 1.5$ and $k_s = 1$ (dashed line); $K = 1$ and $k_s = 1$ (solid line); $K = 1.5$ and $k_s = 2.5$ (dot-dashed line). Also shown are the experimental points (circles).

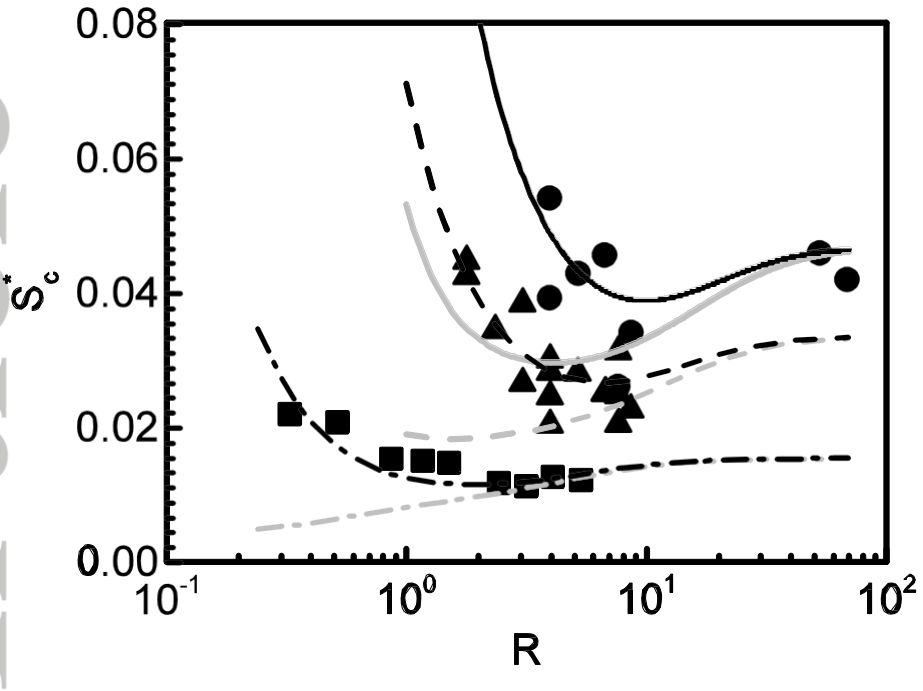

Figure 5. Experimental (symbols) critical Shields parameter with cohesion, S_c^*, as a function of the particle Reynolds number, R, for particle-to-fluid density ratios: $\sigma = 76$ (circles and solid lines); $\sigma = 172$ and 183 (upper triangles and dashed lines); $\sigma = 2083$ (squares and dot- dashed lines). Black and grey lines represent the present theory with and without cohesion.